

A Simple and Effective Use of Object-Centric Images for Long-Tailed Object Detection

Cheng Zhang^{1*} Tai-Yu Pan^{1*} Yandong Li² Hexiang Hu³

Dong Xuan¹ Soravit Changpinyo⁴ Boqing Gong⁴ Wei-Lun Chao¹

¹The Ohio State University ²University of Central Florida

³University of Southern California ⁴Google Research

Abstract

Object frequencies in daily scenes follow a long-tailed distribution. Many objects do not appear frequently enough in scene-centric images (e.g., sightseeing, street views) for us to train accurate object detectors. In contrast, these objects are captured at a higher frequency in object-centric images, which are intended to picture the objects of interest. Motivated by this phenomenon, we propose to take advantage of the object-centric images to improve object detection in scene-centric images. We present a simple yet surprisingly effective framework to do so. On the one hand, our approach turns an object-centric image into a useful training example for object detection in scene-centric images by mitigating the domain gap between the two image sources in both the input and label space. On the other hand, our approach employs a multi-stage procedure to train the object detector, such that the detector learns the diverse object appearances from object-centric images while being tied to the application domain of scene-centric images. On the LVIS dataset, our approach can improve the object detection (and instance segmentation) accuracy of rare objects by 50% (and 33%) relatively, without sacrificing the performance of other classes.

1. Introduction

Detecting objects in the complex daily scenes is a long-standing task in computer vision [22, 73, 54, 16]. With the rapid developments of neural networks [31, 62, 64, 42] and the efforts in data curation [51, 44, 61, 80, 70], state-of-the-art algorithms [30, 59, 52, 56, 50, 49, 2, 89] have achieved remarkable progress in detecting common objects (e.g., cars, humans, etc.). However, for many other objects that appear less frequently or even rarely in daily scenes (e.g., unicycles, bird feeders, etc.), the limited amount of training data leads to a drastic drop in the detection accu-

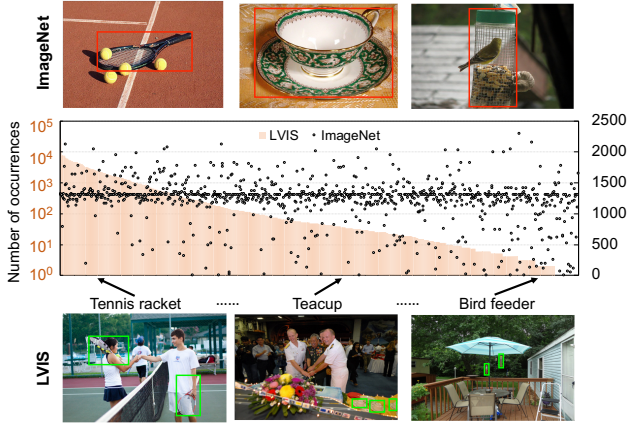


Figure 1. Object frequencies in scene-centric and object-centric images. Orange bars show the number of instances per class in the scene-centric LVIS dataset [25]. Class indices are sorted by the instance numbers. Black dots show the number of images in the object-centric ImageNet datasets [11] for each corresponding class. The two types of images have very different trends of object frequencies. We also show three examples of both datasets, corresponding to frequent, common, and rare classes in LVIS. Red and green boxes indicate the objects. The two types of images have different focuses and object sizes. (Note that, object-centric images are usually not provided with ground-truth bounding boxes.)

racy [25, 72, 87]. Developing algorithms to overcome such a “long-tailed” distribution of object instances in *scene-centric* images [25, 51, 61, 44] has thus attracted a flurry of research interests [65, 76, 48].

The uncommon objects in scene-centric images, however, appear much more frequently in *object-centric* images dedicated to capture the objects of interest (e.g., product images). For example, searching for “unicycle” using Google Images pops out thousands of images of unicycles, more than a hundred times of those included in the LVIS dataset [25] of scene-centric images. The ImageNet dataset [11] for object-centric image classification also contains more than a thousand unicycle images. This is in-

*Equal contributions

deed not surprising, as humans tend to be more interested in taking pictures of rare objects. *Figure 1* further shows the object frequencies of the LVIS and ImageNet datasets: there exists a clear discrepancy. The long-tailed problem in scene-centric images thus may be largely alleviated in object-centric images.

In this paper, we therefore investigate the idea of leveraging object-centric images to improve long-tailed object detection in scene-centric images. Object-centric images have indeed been used in most of the object detection works, but mainly for pre-training the backbone networks [89, 29, 30]. In contrast, we propose to directly include object-centric images in detector training to maximize the potential for boosting the detection accuracy.

Doing so, however, is by no means trivial and we identify two major challenges. First, compared to scene-centric images, where the trained object detector will ultimately be applied, an object-centric image usually contains fewer object instances and has a less complex background; the object instances usually have bigger sizes. These imply a clear domain discrepancy between object-centric and scene-centric images, which may unfavorably hinder knowledge transfer [82, 77]. Second, object-centric images, either from the Web or from datasets like ImageNet, are usually provided with no object bounding boxes (or boxes’ class labels), making it hard to learn accurate object localization.

To resolve these problems, we propose a simple yet effective learning framework for object detection, which is built upon three key components. First, we mosaic multiple object-centric images together to synthesize a scene-centric image, which therefore contains more object instances and classes, more complex background, and smaller instances¹. As shown in our empirical results, such a simple method leads to a notable improvement in detection accuracy for rare objects. Second, we investigate different ways to impute the missing bounding boxes. We find that simply applying the image labels to fixed image locations (*e.g.*, center crops, corner crops, etc.) yields highly robust results. Third, we employ a multi-stage training procedure to leverage these mosaic and label-imputed images. We use them to *fine-tune* a pre-trained object detector to learn better features from diverse object appearances, followed by another stage of training with accurately labeled scene-centric images to adapt the detector to its ultimate application domain.

We validate our framework on the LVIS dataset [25] for long-tailed object detection and instance segmentation. We use object-centric images from ImageNet [11] and from the web. Our approach leads to a significant boost in the accuracy of detecting rare objects, which improves from 13% to over 19% in average precision. For instance segmentation,

¹Mosaicking was exploited in [2, 7], but mainly to combine multiple *scene-centric* images to simulate smaller object sizes or to increase the scene complexity, not to turn object-centric images into scene-centric ones.

our approach even improves the accuracy for common objects. More importantly, compared to several existing methods, our approach improves the accuracy of these classes without sacrificing that of the frequent classes. With its simplicity and effectiveness, we expect our approach to serve as a competitive baseline for long-tailed object detection.

2. Related Work

Long-tailed object detection has attracted increasing attentions recently. The main problem is the drastically low detection accuracy for object classes that rarely appears. Most of the works develop new training strategies or objective functions to overcome the problem [25, 36, 48, 55, 76, 65, 75, 67, 58, 78]. Wang et al. [75] found that the major drop of detection accuracy comes from mis-classification, suggesting that methods for class-imbalanced classification (*e.g.*, re-weighting, re-sampling) are also applicable to long-tailed object detection [41, 24, 51, 70, 72, 85, 5, 10, 6, 27, 10, 4, 39, 27]. We investigate an alternative direction to address the problem, by not developing new objectives but exploiting the availability of abundant object-centric images.

Weakly-supervised, semi-supervised object detection learns or improves object detectors using images with weak supervision (*e.g.*, image-level labels) [46, 18, 71, 1, 13] or without supervision [38, 47, 18, 63, 89]. Most of them either leverage scene-centric images or detect only a relative small numbers of common classes (like those classes in Pascal VOC [14], MSCOCO [51], or ILSVRC [60]). Our work can be seen as weakly supervised object detection, but we focus on a much challenging long-tailed detection task with more than 1,000 object classes. Also, we leverage object-centric images, which have very different appearances and layouts from scene-centric images. The closest to ours is [55], which uses YFCC-100M [70] (Flickr images) to improve the detection accuracy on LVIS [25]. YFCC-100M mixes object-centric and scene-centric images and contains non-negligible label noises. Thus, [55] employs more sophisticated data pre-processing and pseudo-labeling steps, yet our approach achieves a much higher accuracy.

Some other works use object-centric images to expand the label space of a object detector [43, 33, 69, 68, 34, 35, 57]. However, most of them only use these images to learn the last fully-connected layer for classification, not to improve the feature extractor. Moreover, we show that object-centric images can improve not only object detection, but also instance segmentation.

Data augmentation improves model training by enlarging the training set, *e.g.*, by applying data transformations to the original training data [88, 2, 81, 32, 21, 7, 84, 12, 20, 52, 9, 86]. We find that, a simple stitching trick over object-centric images is highly effective as a data augmentation method for object detection in scene-centric images.



(a) Scene-centric



(b) Object-centric

Figure 2. Scene-centric images vs. object-centric images. We show one image for each type. Both of them contain unicycles inside. (a) A scene-centric image is taken to capture a scene (*e.g.*, street views), which often contains multiple small object instances (and classes) in a complex background. (b) An object-centric image is specifically taken to capture the object(s) of interest.

3. Scene-Centric vs. Object-Centric Images

Images taken by humans in their daily lives can roughly be categorized into object-centric and scene-centric images. The former captures objects of interest (*e.g.*, cats, food) and usually contains just one salient object class whose name can be used as the image label. The latter captures a scene (*e.g.*, street views, sightseeing) and usually contains multiple object instances of different classes in a complex background. **Figure 2** shows one example of each type.

Recent works of object detection mainly study scene-centric images [51, 25, 61], probably because they are both challenging and applicable to a wide range of real applications. For instance, a self-driving car must be able to detect objects such as other cars and pedestrians in street scenes so as to prevent collision and plan safe routes [80, 8, 19]. However, as scene-centric images are not intended to capture specific objects, *object frequencies in our daily lives will likely be reflected in the images*. As such, the learned object detector will have a hard time detecting rare objects because it just has not seen sufficient instances to understand the objects' appearances, shapes, variations, etc.

In contrast, humans tend to take object-centric images to capture interesting (and likely uncommon, rare) objects, especially during specific events or activities (*e.g.*, bird watching, car shows). Therefore, even a rare object in our daily lives may have thousands of unique images online.

Discrepancy in object frequencies. To illustrate this difference, we compare object frequencies captured in the ImageNet [11] and LVIS (v0.5) [25] datasets. The former retrieved images from the Web by querying several image search engines using the object class names (thus mostly object-centric). The later used images from MSCOCO [51], which gathered images of daily scenes that contain common objects in the natural context (thus mostly scene-centric).

The full ImageNet dataset contains over 21,000 unique object classes, whereas LVIS has around 1,230. Using the

WordNet synsets [53] (*e.g.*, banana.n.02), we are able to match 1,016 classes between them. **Figure 1** shows the number of object instances per class in LVIS (for those 1,016 classes) and the number of images per corresponding class in ImageNet. As shown, *the two datasets (data sources) have a large discrepancy in the trend of object frequencies*. Specifically, ImageNet has a more balanced distribution across classes. Even for rare classes in LVIS (those with < 10 training images), ImageNet usually contains more than 1,000 images. We argue that, such a discrepancy indeed offers a great opportunity to resolve the long-tailed problem in scene-centric images with the help of object-centric images.

Discrepancy in image appearances and contents. Beyond frequencies, these two types of images also have other, less favorable discrepancies. The obvious one is the number of object instances per image. LVIS on average has **12.1** labeled object instances per image (the median number of instances per image is **6**). While most of the ImageNet images are not annotated with object bounding boxes, according to a subset of image used in the ILSVRC detection challenge [60], each image has **2.8** object instances. The larger number of object instances, together with the intention behinds the images, implies that scene-centric images also have *smaller* objects in size and more complex backgrounds. This type of discrepancies, contrast to that in object frequencies, is not favorable for leveraging the object-centric images, and may lead to negative transfer [82, 77].

4. Overall Framework

To better leverage the object-centric images for object detection, we present a novel learning framework, which includes **three simple² yet effective components** to handle

- (a) the domain gap between the two image sources;
- (b) the missing bounding box labels;
- (c) the integration of both image sources for training.

Figure 3 gives an illustration of our framework. Concretely, the framework begins with pre-training an object detector using the accurately labeled scene-centric images. Any object detector can be applied. Without loss of generality, we will focus on faster-RCNN [59], one of the most popular object detectors in the literature. The pre-trained object detector serves for two purposes: it can help impute the missing boxes in object-centric images; it will be used as the initialization for training with the object-centric images.

To turn object-centric images into training examples for object detection, we must handle both (a) and (b). We post-

²We claim our approach to be “simple” as it employs simple methods to address the challenges of leveraging object-centric images. Pseudo-labeling is an essential step to use weakly-supervised data, and we apply simple fixed locations. We apply mosaic and two-stage training (*i.e.*, fine-tuning on the application domain) to bridge the domain gap, instead of applying sophisticated methods like domain adversarial training [17].

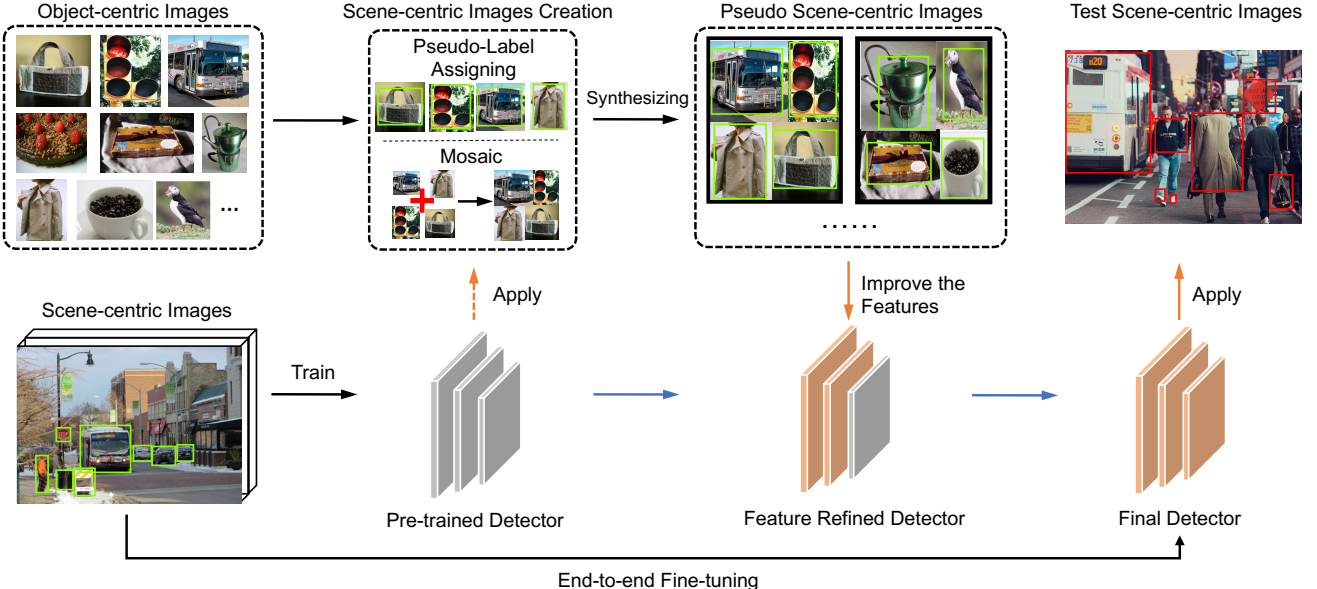


Figure 3. **Our framework for learning object detectors with object-centric and scene-centric images.** On the one hand, we pre-train a detector using available labeled scene-centric images. On the other hand, we assign the image label of each object-centric image to a set of pseudo ground-truth bounding boxes inside, and stitch multiple images together to form a training image (named a pseudo scene-centric image) for detection. We then use these pseudo scene-centric images to fine-tune the pre-trained detector to learn better features, followed by another stage of training with the labeled scene-centric images to ensure the detector’s ultimate detection and localization performance. The green boxes indicate the (pseudo) ground truths; the red boxes indicate the detection results.

pone the details of these two components to [section 5](#). For now, let us assume that we have annotated the object-centric images with pseudo ground-truth boxes and class labels exactly like the labeled scene-centric images. To differentiate from the original object-centric images, we call these new images *pseudo scene-centric images* (see [Figure 3](#)).

These pseudo scene-centric images may still have domain gap from scene-centric images, to which the learned object detector will ultimately be applied. Besides, the pseudo ground-truth bounding boxes likely contain noises (*e.g.*, wrong box locations). To effectively learn better features from these images (especially for the rare objects) while not sacrificing the detector’s ultimate accuracy on identifying and locating objects, we propose to learn³ the object detector in multiple stages, first using pseudo scene-centric images and then using scene-centric images. In what follows, we begin with a brief review of object detection, and then describe the multi-stage learning procedure.

Backgrounds on object detection. An object detector has to identify objects with their class names and locate each of them by a bounding box. Taking faster-RCNN [59] as an example, the detector first generates a set of candidate object proposals (usually around 512) that likely contain objects of interest. This is done by the so-called region proposal network (RPN) [59]. Faster-RCNN then goes through

each proposal to identify its class label and refine the proposed bounding box location and size.

The entire faster-RCNN is learned with three loss terms

$$\mathcal{L} = \mathcal{L}_{\text{rpn}} + \mathcal{L}_{\text{cls}} + \mathcal{L}_{\text{reg}}, \quad (1)$$

where \mathcal{L}_{rpn} is for RPN training, \mathcal{L}_{cls} is for multi-class classification (usually a cross-entropy loss), and \mathcal{L}_{reg} is for box refinement (usually a regression loss).

Multi-stage training. Our multi-stage training begins with learning the detector using the labeled scene-centric images. All the three loss terms in [Equation 1](#) are involved.

Next, we fine-tune the detector using the pseudo scene-centric images that are generated from object-centric images (see [section 5](#)). Concretely, we perform RPN on each image to create 512 proposals and assign each proposal a class label (can be background) according to its proximity to the annotated boxes of the image. We then use these labeled proposals to fine-tune the detector using only \mathcal{L}_{cls} . In other words, we do not optimize \mathcal{L}_{rpn} or \mathcal{L}_{reg} , which makes sense as the annotated boxes in pseudo scene-centric images are likely noisy. *Note that, we do not freeze any layers of the detector⁴; any network parameters that affect \mathcal{L}_{cls} , especially those in the backbone feature network, can be updated.*

³More precisely, fine-tune from the pre-trained detector.

⁴Except for the batch-norm layers [37] in the backbone feature network which are kept frozen by default.

After this stage, we then fine-tune the detector again with the labeled scene-centric images, just like the first stage. All the three loss terms in [Equation 1](#) are optimized. This stage serves for two purposes. First, it helps align the three loss terms, updating the RPN and the regression sub-network that were kept intact in the previous stage. Second, it adapts the detector back to real scene-centric images.

5. Creating Pseudo Scene-Centric Images

In this section, we will focus on the missing piece of our framework in [section 4](#): how to generate the pseudo scene-centric images from object-centric images? Our goal here is to create images that are more like scene-centric images and annotate them with pseudo ground truths. In what follows, we begin with how to collect object-centric images.

5.1. Collecting object-centric images

We collect object-centric images from two resources: ImageNet [11] and Google Image. We use the full ImageNet dataset with 21,842 object classes, and keep those classes whose WordNet synset names [53] match those in the LVIS dataset [25]. This gives us 1,025 overlapped classes, with in total 1,243,359 image URLs (860,989 images from 1,016 classes are downloadable). We further wrote a crawler to retrieve 100 images from Google Images for all the 1,230 LVIS classes, using their synset names and descriptions as the queries.

5.2. Assigning pseudo-labels

Each object-centric image has one object class label, but no bounding box annotations. Some images may contain multiple object instances and classes, in which the class label only tells the most salient object. Our goal here is thus to create a set of pseudo ground-truth bounding boxes that likely contain the object instances for each image, and assign each of them a class label, such that we can use the image to directly train an object detector.

There are indeed many works on doing so, especially those for weakly-supervised or semi-supervised object detection [46, 71, 1, 13, 47, 18, 55]. The purpose of this sub-section is therefore not to propose a new way to compare with them, but to investigate approaches that are more effective and efficient in a large-scale long-tailed setting. Specifically, we investigate four methods that do not learn an extra detector or proposal network beyond the pre-trained one. [Figure 4](#) illustrates the difference of these methods.

Fixed locations. We simply set some fixed locations of an object-centric image as the pseudo ground-truth boxes, regardless of the image content. The hypothesis is that many of the object-centric images may just focus on one object instance whose location is likely in the middle (*i.e.*, just like those in [23, 15]). Specifically, we investigate the combination of the whole image, the center crop, and the four corner

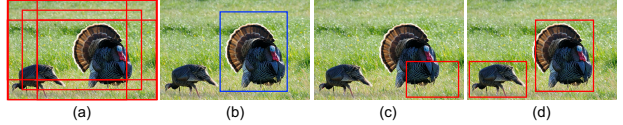


Figure 4. A comparison of pseudo-label generation: (a) fixed locations, (b) trust the detector, (c) trust the detector + image labels, (d) localization by region removals. The image label is “turkey,” a rare class in LVIS. **Red** boxes indicate true labels; **blue** boxes indicate wrong labels (by the detector).

crops: in total **6** boxes per image. The height and width of the crops are 80% of the original image. We assign each box the image label.

Trust the pre-trained detector. We apply the pre-trained detector learned with the scene-centric images to the object-centric images, and treat the detected boxes and predicted class labels as the pseudo-labels. Specifically, we keep all the detection of confidence scores $> 0.5^5$. We apply non-maximum suppression (NMS) within the detected boxes of each class using an IoU (intersection-over-union) threshold 0.5. By doing so, every image will have boxes of different sizes and locations, and labeled with different classes.

Trust the pre-trained detector and image label. One potential drawback of the method above is its tendency to assign high-frequency labels, a notorious problem in class-imbalanced learning [79, 39, 65]. For instance, if “bird” is a frequent class and “eagle” is a rare class, then the detector may correctly locate an “eagle” in the image but assign a label “bird” to it. To resolve this, we combine the detector’s prediction with the known image label. Concretely, from the top detected boxes (with high confidence scores) we select the one whose class probability of the image label is the highest to be the only pseudo ground-truth box, labeled with the image label. In other words, a box initially labeled as “bird” may be replaced by the label “eagle” if “eagle” is the image label. The rationale here is that the image label indicates that *at least* one such object appears in the image.

Localization by region removal (LORE). We investigate yet another method to resolve the aforementioned problem, taking the following intuition: an image classifier should fail to predict the correct label if the true object regions are removed. To this end, we first train a ResNet-50 [28] image classifier using our object-centric image pool⁶. We then collect the pre-trained detector’s detection, trusting the box locations but not the class labels. We sort these boxes by how much removing each boxed region alone reduces the image classifier’s confidence on the image label. We then remove these boxed regions *in turn* until the classifier fail to

⁵Selecting a threshold per class with respect to its class size (*i.e.*, a rare class has a lower threshold) needs a suitable function that maps the class size to the threshold, which is still an open problem.

⁶That is, we train the classifier with these images, and then apply this classifier back to these images (after some regions are removed).

predict the true label. The bounding boxes of the removed regions are then collected as the pseudo ground truths for the image. We assign each box the image label. See the supplementary material for details.

5.3. Synthesizing pseudo scene-centric images

We investigate a very simple approach, namely image mosaic. We stitch multiple object-centric images together to obtain a new image that contains more object instances and classes, smaller object sizes, and more complex background. Specifically, we stitch 2×2 images together, which are sampled either randomly within a class, or randomly from the entire image pool. We do not apply sophisticated stitching tools like [3, 83, 26] but simply concatenate these object-centric images one-by-one. The resulting images are thus more like *mosaics*, having artifacts along the stitched boundaries. See Figure 3 for an illustration.

6. Experiments

6.1. Setup

Long-tailed datasets and metrics. We evaluate our proposed framework on the LVIS v0.5 instance segmentation benchmark [25]⁷ which contains 1,230 entry-level object categories with around 2 million high-quality annotations. The training set contains all the classes with a total of 57,623 images; the validation set contains 830 classes with a total of 5,000 images. The categories are naturally long-tailed distributed which are divided into three groups based on the number of training images per class: rare (1-10 images), common (11-100 images), and frequent (>100 images). We report all results on the validation set. We adopt the standard mean average precision (AP) metric in LVIS [25]. We specifically focus on the object detection task with the standard bounding box evaluation, AP^b . The performance on the rare, common, and frequent classes (AP_r^b , AP_c^b , AP_f^b) are reported as well. We also experiment our approach on instance segmentation.

Object-centric data sources. As mentioned in subsection 5.1, we use images from two sources: ImageNet [11] and Google crawler. ImageNet is a standard image classification benchmark. Most people use its 1,000 categories version in ILSVRC [60] and, more recently, treat it as the standard data for backbone network pre-training in various computer vision tasks such as object detection and segmentation. The full version of ImageNet has 21,842 classes. In LVIS and ImageNet, each category can be identified by a unique WordNet synset ID [53]. We are able to match 1,016 LVIS classes and retrieve the corresponding images from ImageNet as their object-centric images (in total, 860,989

⁷Many algorithms on long-tailed recognition report results on this version (*i.e.*, v0.5), allowing us to make direct comparisons. Please refer to the supplementary material for more results and discussion.

images). On the other hand, we retrieve images via Google by querying with class names and descriptions provided by LVIS. Such a text-to-image search returns hundreds of iconic images and we take the top 100 for each of the 1,230 classes to augment the object-centric pool.

Implementations. We use faster-RCNN [59] as our base detector and ResNet-50 [31] with a Feature Pyramid Network (FPN) [49] as the backbone, which is pre-trained on ImageNet-1K [60]. The base detector is then trained on the LVIS training set with repeated factor sampling, following the standard training procedure in [25]. In order to fairly compare with our fine-tuning results, we further extend the training process with another 90K iterations and select the checkpoint with the best AP^b as **faster-RCNN***. The following experiments are initialized from faster-RCNN*.

For our proposed framework, we first fine-tune faster-RCNN* with our pseudo scene-centric images (generated from object-centric images, see section 5) using only the classification loss. We then end-to-end fine-tune the entire model using the LVIS training set with all losses (see section 4). All steps are trained with stochastic gradient descent with a mini-batch size of 16, momentum of 0.9, weight decay of 0.0001, and learning rate of 0.0002.

Baselines. We compare to the following baselines:

- **Self-training.** Self-training is a strong baseline for semi-supervised learning [45]: the current model (*e.g.*, faster RCNN*) predicts labels on the unlabeled data, turns the high confident ones to hard labels, and fine-tunes on top of them together with the original training data. We use the basic version of self-training to replace our first stage fine-tuning on the base detector. That is, faster RCNN* is used to create pseudo-labels on the object-centric images, exactly like the “trust the pre-trained detector” or the “trust the pre-trained detector and image label” methods (cf. subsection 5.2). We then train the base detector using them for 90K iterations with *all three loss terms*. We finally end-to-end fine-tune the detector using the original LVIS images.

- **Single-stage training.** We combine our two-stage framework into one. Specifically, we jointly learn with LVIS images and pseudo scene-centric images. The later only contribute to the classification loss. Our setup is 50% data from each source per batch. We tried other ratios but did not see notable differences.

- **DLWL** [55]. A state-of-the-art method that leverages extra unlabeled images from the YFCC dataset [70].

For self-training and single-stage training, we perform 2×2 mosaic to turn the pseudo-labeled object-centric images into pseudo scene-centric images.

Our variants. We investigate several variants of our approaches. First, we compare using ImageNet images (1,016 classes) and ImageNet + Google images (1,230 classes). Second, we compare with or without object-centric image

Table 1. **Comparison of object detection on LVIS v0.5 dataset.** **OCIs:** the source of object-centric images (IN: ImageNet, G: Google). **Mosaic:** the number of images being stitched. **Hybrid:** ✓ means stitching images from different classes. **P-GT:** ways to generate pseudo-labels/-ground-truths (F: six fixed locations, D: “trust the pre-trained detector”, D†: “trust the pre-trained detector and image label”, S: “one single box of the whole image”, and L (LORE): “localization by region removal”). The best result per column is in bold font.

Method	OCIs	Mosaic	Hybrid	P-GT	AP ^b	AP ₅₀ ^b	AP ₇₅ ^b	AP _r ^b	AP _c ^b	AP _f ^b
faster RCNN	-	-	-	-	23.17	38.94	24.06	12.64	22.40	28.33
faster RCNN*	-	-	-	-	23.35	39.15	24.15	12.98	22.60	28.42
Vanilla self-training	IN	2 × 2	✓	D	23.04	38.97	23.72	13.93	21.51	28.14
	IN	2 × 2	✓	D†	23.62	39.34	25.11	13.84	22.98	28.31
Single-stage training	IN	2 × 2	✓	F	22.48	38.63	23.46	14.39	21.26	27.25
Multi-stage (Ours)	IN	✗	✗	F	23.81	39.97	24.89	15.18	22.91	28.39
	IN	✗	✗	F	24.42	40.93	25.36	18.15	23.12	28.56
	IN	2 × 2	✓	F	24.53	40.75	25.58	18.87	23.07	28.61
	IN	2 × 2	✓	D	23.28	38.70	24.55	13.29	22.50	28.24
	IN	2 × 2	✓	D†	23.09	38.77	24.15	11.84	22.53	28.29
	IN	2 × 2	✓	S	24.29	40.42	25.17	17.94	22.91	28.54
	IN	2 × 2	✓	L	24.47	41.01	25.17	18.26	23.15	28.61
	IN+G	2 × 2	✓	F	24.66	41.08	25.80	19.47	23.35	28.37

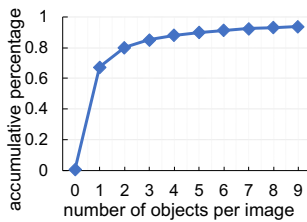


Figure 5. **Number of objects found per object-centric image via Localization by Region Removal (LORE).** Y-axis is the accumulative percentage of how many images having boxes no more than the X-axis number.

stitching. Third, for mosaicking, we compare stitching images from the same classes (so the mosaic artifacts can be reduced) or from randomly drawn images. Forth, we compare different ways to generate pseudo ground-truth box labels (see subsection 5.2).

6.2. Experimental results on object detection

Main results. We report our main results in Table 1. Our multi-stage approach with object-centric images outperforms faster-RCNN* (and faster-RCNN) substantially. Specifically on AP_r^b for rare classes, our best result 19.47% is $\sim 6.5\%$ higher than faster-RCNN*, justifying our motivation: *object-centric images that are resistant to the long-tailed nature of object frequencies can be a valuable source to improve object detection on scene-centric images*. Next, we provide more detailed analyses.

Mosaicking is useful (red in Table 1). A simple image 2 × 2 stitching leads to a notable gain: $\sim 3.0\%$ at AP_r^b, supporting our claim that making object-centric images similar to scene-centric images is important. Indeed, according to section 3, a 2 × 2 stitched image will have around 12 objects, very close to that in LVIS images. By further comparing how to select images for stitching (green in Table 1), we see that using images from multiple classes helps.

Fixed-location boxes are strong (blue in Table 1). By comparing different ways for pseudo-labels, we found that the very simple fixed-location boxes leads to the strongest results. The LORE approach via localization by region removal performs on a par. Both methods significantly outperform “trust the pre-trained detector”. This is probably due to the poor pre-trained detector’s accuracy on detecting rare classes: it just cannot identify rare classes from the images to construct pseudo-labels. We also found that both LORE and six fixed locations outperform the single box surrounding the whole object-centric image (S), demonstrating that finer-grained locations from either LORE or F are beneficial. They are supposed to more accurately capture the target objects (those of the image labels) in the image.

To analyze why fixed locations work so well, we check the numbers of boxes LORE finds per image: LORE keeps removing object regions until the classifier fails to classify the image; the number of regions it found thus is an estimate of how many target objects are in an image. Figure 5 shows the accumulative number of images whose object numbers are no more than a threshold: $\sim 70\%$ of images have just one object instance, suggesting that it may not be necessary to locate and separate object instances in pseudo-labeling.

Single-stage training and self-training. Our approach using fixed-location boxes notably outperforms both baselines, which tells two messages. First, pre-trained detectors’ class predictions are not reliable for assigning pseudo-labels. Second, a multi-stage training strategy by first learning with object-centric images and then scene-centric images better ties the detector to its final application domain.

The amount of object-centric data (brown in Table 1). While ImageNet-21K images can only cover 1,016 classes of the LVIS v0.5 dataset, we can retrieve 100 images for

Table 2. Comparisons of object detection on LVIS v0.5 using different extra data sources. G: Google Images. IN: ImageNet.

Method	Data	AP ^b	AP _r ^b	AP _c ^b	AP _f ^b
faster RCNN*	-	23.35	12.98	22.60	28.42
DLWL [55]	YFCC	22.14	14.21	-	-
Ours	Flickr	23.55	15.62	22.25	28.36
	G	24.04	17.84	22.47	28.49
	IN	24.53	18.87	23.07	28.61
	IN+G	24.66	19.47	23.35	28.37

Table 3. Performance of object detection on the 176 overlapped classes between ImageNet-1K (ILSVRC) and LVIS v0.5.

	AP ^b	AP _r ^b	AP _c ^b	AP _f ^b
# Category	176	21	84	71
faster RCNN*	26.05	14.78	23.92	31.16
Ours	27.12	20.11	24.61	32.17

other classes via search engines like Google Images. By including them into our framework, we see yet another 0.6% gain at rare classes (AP_r^b).

Does the quality of data source matter? DLWL [55] uses YFCC-100M [70], an even larger data source than ImageNet, to augment the training. YFCC-100M images are mainly collected from Flickr, which mixes object-centric and scene-centric images and contains higher label noises. DLWL [55] therefore develops sophisticated data pre-processing and pseudo-labeling steps. In contrast, we specifically leverage *object-centric* images that have higher object frequencies and usually contain only single object classes (the image labels), leading to a much simpler approach. As shown in Table 2, our method outperforms DLWL by a large margin: > 5.0% at AP_r^b. We argue that our ways of strategically collecting object-centric images and stitching them to make them scene-centric alike make the difference. The fact that we identify a better data source should not lead to an impression that we merely solve a simpler problem, but an evidence that selecting the right data source is crucial to simplify a problem.

For a fair comparison to [55] in terms of the algorithms, we also investigate Flickr images. Since [55] does not provide their processed data, we try our best to crawl Flickr images (100 per class) and re-train our algorithm. We achieve 23.55/15.62 AP^b/AP_r^b, better than DLWL. Using pure Google images beyond ImageNet can achieve 24.04/17.84. Our novelties and contributions thus lie in both the algorithm and the direction we investigate. The latter specifically leads to simpler solutions but higher accuracy.

Image reusing at detector training. To justify that our improvements do not simply come from having more object-centric images, but the way to use them, we look at the ILSVRC object classes that are overlapped with LVIS classes. We found in total 176 of them in the LVIS vali-

Table 4. Object detection on LVIS v0.5. COCO: using COCO images for backbone pre-training. [58]: incorporating the balanced loss developed in [58].

Method	COCO	[58]	AP ^b	AP _r ^b	AP _c ^b	AP _f ^b
EQL [65]			23.30	-	-	-
			22.60	-	-	-
			25.96	17.65	25.75	29.54
			24.40	16.90	24.30	27.70
Ours			24.66	19.47	23.35	28.37
			25.76	16.04	25.44	30.05
			26.16	19.59	25.20	29.98
			27.65	18.94	27.59	31.21

dation set. For these classes, the ImageNet images that we use are indeed already seen by the baseline detector: they were used in the backbone pre-training. Surprisingly, as shown in Table 3, our learning strategy still leads to a significant gain for all these classes. This not only justifies the efficacy of our approach, but also suggests that the detector, after training with scene-centric images, may have forgotten the discriminative knowledge it has learned in its backbone, essentially an instance of catastrophic forgetting [40].

Comparison to state-of-the-art methods. We compare our approach to several existing methods that propose advanced training strategies and losses but do not use extra object-centric images in Table 4. Our approach achieves comparable or even better results, especially on rare classes, suggesting that it is a valuable add-on to the literature.

Compatibility with existing efforts. Our approach is compatible with recent efforts in better backbone pre-training [48] and class-balanced training objectives [58]. For instance, following BAGS [48] to pre-train the backbone using COCO images, we achieve an improved 25.76 AP^b (cf. Table 4). Further adding BALMS [58] to the final-stage training boosts AP^b to 27.65, showing the compatibility of our approach to the existing ones.

Qualitative results. We show qualitative visualizations of the detected objects on LVIS v0.5 validation set in Figure 6. Our approach consistently outperforms the baseline, especially on detecting rare objects; *e.g.*, distinguishing a rare class (*e.g.* “vulture”) from a frequent one (*e.g.*, “bird”).

6.3. Experimental results on instance segmentation

Our method can be applied to instance segmentation as well. The overall procedure is the same: (1) we prepare pseudo box labels; (2) in training with object-centric image, we only optimize the *object classification* loss, not the other losses like segmentation. The model only learns to do instance segmentation from LVIS images. For this experiment, we apply a mask-RCNN [30] model. Table 5 shows the results: *the compared baselines are not using object-centric images*. We again see a significant gain against the

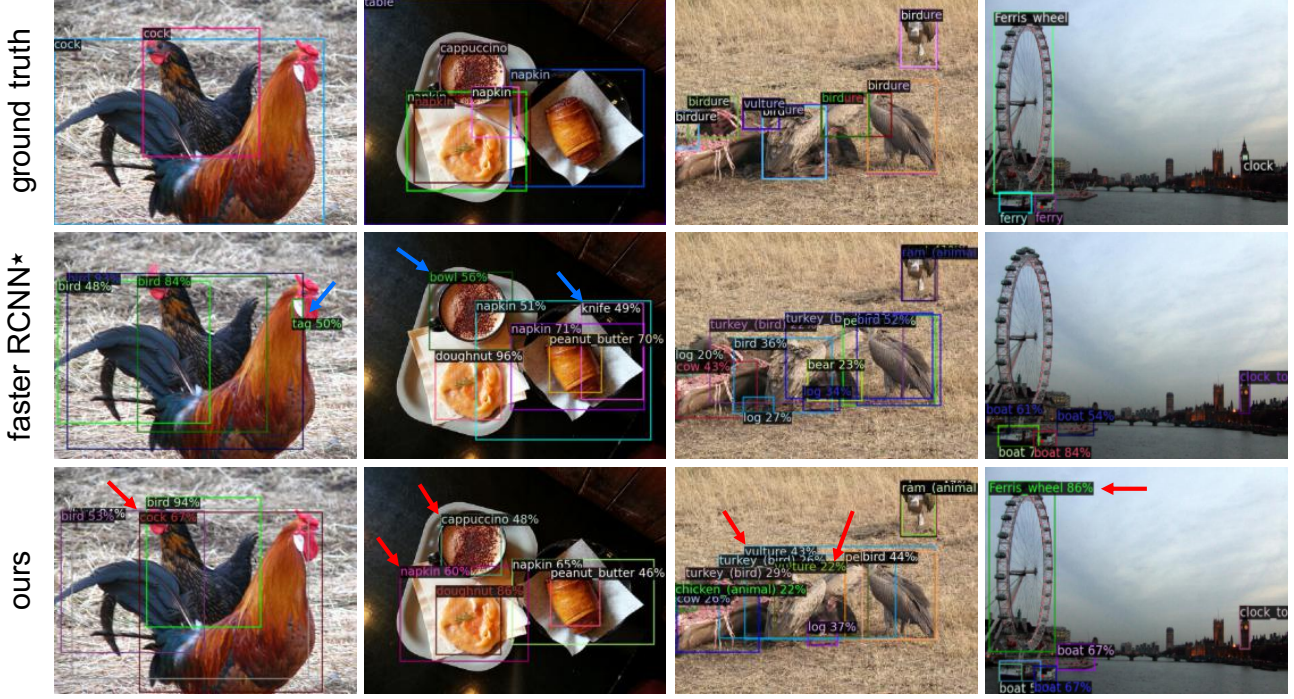


Figure 6. **Qualitative results of object detection on LVIS v0.5 dataset.** Our approach can largely improve the detection accuracy of rare classes. We superimpose red arrows to show where we did right while the baseline did wrong (blue arrows).

Table 5. **Instance segmentation on LVIS v0.5.** We use mask-RCNN [30] as our model and show mAP of instance segmentation. + [58] means including its balanced loss in the final training stage.

Method	AP	AP _r	AP _c	AP _f
mask RCNN [25]	24.38	15.98	23.96	28.27
EQL [65]	22.80	11.30	24.70	25.10
LST [36]	23.00	-	-	-
Forest RCNN [78]	25.60	18.30	26.40	27.60
BALMS [58]	27.00	19.60	28.90	27.50
Ours	26.14	18.55	26.56	28.65
Ours + [58]	27.79	21.16	28.61	29.42

mask-RCNN baseline, for both rare and common classes, even if we do not have segmentation labels on object-centric images. This seems to support the claim by [75]: even for detection and segmentation, the long-tailed problem mainly affects the classification sub-network. Compared to other existing methods, we outperform many of them. See the supplementary material for details.

7. Discussion

Our contributions lie in a novel direction — *leveraging object-centric images to improve long-tailed object detection*. While most existing works focus on *algorithm design* to directly learn from long-tailed data, we propose an orthogonal way to address it, by investigating what *data*

sources may simplify the problem. After all, the success of machine learning depends not only on algorithm design, but also on data preparation.

While leveraging auxiliary data to improve *common* object detection has been studied (see section 2), existing works mostly assume access to well prepared auxiliary data that are captured in a similar domain to the test data and contain sufficient object instances. For real-world *long-tailed* object detection, however, even identifying and collecting the suitable auxiliary data is challenging. One of our novelties is thus the use of *object-centric* images as the auxiliary data, which contains sufficient object instances but captured in a different domain. Using a suitable data source (like ImageNet that more focuses on single object types) is another strength of our paper, as evidenced by the notable accuracy gap against [55], which uses YFCC [70].

To establish the new direction and demonstrate its feasibility *so that future works can easily build upon*, we intentionally make our pipeline and algorithms straightforward and simple. We identify two main challenges of leveraging object-centric images — domain gaps and the lack of object labels — and investigate simple solutions like fixed box locations, mosaicking, and multi-stage training. More sophisticated techniques in self-training and weakly-supervised and semi-supervised learning may be incorporated as well. *The facts that (a) our solutions have achieved comparable accuracy to state-of-the-art methods in long-tailed detec-*

tion and (b) many existing techniques can be easily plugged into our pipeline further justify the feasibility and potential of the proposed direction.

8. Conclusion

Long-tailed object detection is challenging not only because it is a highly-imbalanced machine learning problem, but also because real object frequencies really follow it: it is just so hard to see rare objects in daily scenes. In this paper, we took a new perspective to this problem by investigating a different image domain, object-centric images. We found in this domain, rare objects may simply have tons of images, essentially an opportunity that we can take advantage of to resolve long-tailed detection. To this end, we proposed a novel framework to learn a detector with object-centric images, consisting of three surprisingly simple but effective components to mitigate the domain gap. Our results are encouraging, improving the baseline model by a large margin on not only detecting but also segmenting rare objects. We hope that our study can attract more attentions in using this already available but less explored source, object-centric images, to overcome the long-tailed problem.

Acknowledgments

We are thankful for the generous support of computational resources by Ohio Supercomputer Center and AWS Cloud Credits for Research.

References

- [1] Hakan Bilen and Andrea Vedaldi. Weakly supervised deep detection networks. In *CVPR*, 2016. [2](#) [5](#)
- [2] Alexey Bochkovskiy, Chien-Yao Wang, and Hong-Yuan Mark Liao. Yolov4: Optimal speed and accuracy of object detection. *arXiv preprint arXiv:2004.10934*, 2020. [1](#), [2](#)
- [3] Matthew Brown and David G Lowe. Automatic panoramic image stitching using invariant features. *IJCV*, 74(1):59–73, 2007. [6](#)
- [4] Mateusz Buda, Atsuto Maki, and Maciej A Mazurowski. A systematic study of the class imbalance problem in convolutional neural networks. *Neural Networks*, 106:249–259, 2018. [2](#)
- [5] Kaidi Cao, Colin Wei, Adrien Gaidon, Nikos Arechiga, and Tengyu Ma. Learning imbalanced datasets with label-distribution-aware margin loss. In *NeurIPS*, 2019. [2](#)
- [6] Nitesh V Chawla, Kevin W Bowyer, Lawrence O Hall, and W Philip Kegelmeyer. Smote: synthetic minority oversampling technique. *Journal of artificial intelligence research*, 16:321–357, 2002. [2](#)
- [7] Yukang Chen, Peizhen Zhang, Zeming Li, Yanwei Li, Xiangyu Zhang, Gaofeng Meng, Shiming Xiang, Jian Sun, and Jiaya Jia. Stitcher: Feedback-driven data provider for object detection. *arXiv preprint arXiv:2004.12432*, 2020. [2](#)
- [8] Marius Cordts, Mohamed Omran, Sebastian Ramos, Timo Rehfeld, Markus Enzweiler, Rodrigo Benenson, Uwe Franke, Stefan Roth, and Bernt Schiele. The cityscapes dataset for semantic urban scene understanding. In *CVPR*, 2016. [3](#)
- [9] Ekin D Cubuk, Barret Zoph, Dandelion Mane, Vijay Vasudevan, and Quoc V Le. Autoaugment: Learning augmentation strategies from data. In *CVPR*, 2019. [2](#)
- [10] Yin Cui, Menglin Jia, Tsung-Yi Lin, Yang Song, and Serge Belongie. Class-balanced loss based on effective number of samples. In *CVPR*, 2019. [2](#)
- [11] Jia Deng, Wei Dong, Richard Socher, Li-Jia Li, Kai Li, and Li Fei-Fei. Imagenet: A large-scale hierarchical image database. In *CVPR*, 2009. [1](#), [2](#), [3](#), [5](#), [6](#)
- [12] Terrance DeVries and Graham W Taylor. Improved regularization of convolutional neural networks with cutout. *arXiv preprint arXiv:1708.04552*, 2017. [2](#)
- [13] Santosh K Divvala, Ali Farhadi, and Carlos Guestrin. Learning everything about anything: Webly-supervised visual concept learning. In *CVPR*, 2014. [2](#), [5](#)
- [14] Mark Everingham, Luc Van Gool, Christopher KI Williams, John Winn, and Andrew Zisserman. The pascal visual object classes (voc) challenge. *IJCV*, 88(2):303–338, 2010. [2](#)
- [15] Li Fei-Fei, Rob Fergus, and Pietro Perona. Learning generative visual models from few training examples: An incremental bayesian approach tested on 101 object categories. In *CVPR*, 2004. [5](#)
- [16] Pedro F Felzenszwalb, Ross B Girshick, David McAllester, and Deva Ramanan. Object detection with discriminatively trained part-based models. *TPAMI*, 32(9):1627–1645, 2009. [1](#)
- [17] Yaroslav Ganin, Evgeniya Ustinova, Hana Ajakan, Pascal Germain, Hugo Larochelle, François Laviolette, Mario Marchand, and Victor Lempitsky. Domain-adversarial training of neural networks. *JMLR*, 17(1):2096–2030, 2016. [3](#)
- [18] Jiyang Gao, Jiang Wang, Shengyang Dai, Li-Jia Li, and Ram Nevatia. Note-rcnn: Noise tolerant ensemble rcnn for semi-supervised object detection. In *ICCV*, 2019. [2](#), [5](#)
- [19] Andreas Geiger, Philip Lenz, Christoph Stiller, and Raquel Urtasun. Vision meets robotics: The kitti dataset. *The International Journal of Robotics Research*, 2013. [3](#)
- [20] Robert Geirhos, Patricia Rubisch, Claudio Michaelis, Matthias Bethge, Felix A Wichmann, and Wieland Brendel. Imagenet-trained cnns are biased towards texture; increasing shape bias improves accuracy and robustness. In *ICLR*, 2019. [2](#)
- [21] Georgios Georgakis, Arsalan Mousavian, Alexander C Berg, and Jana Kosecka. Synthesizing training data for object detection in indoor scenes. *arXiv preprint arXiv:1702.07836*, 2017. [2](#)
- [22] Ross Girshick, Jeff Donahue, Trevor Darrell, and Jitendra Malik. Rich feature hierarchies for accurate object detection and semantic segmentation. In *CVPR*, 2014. [1](#)
- [23] Gregory Griffin, Alex Holub, and Pietro Perona. Caltech-256 object category dataset. 2007. [5](#)
- [24] Yandong Guo, Lei Zhang, Yuxiao Hu, Xiaodong He, and Jianfeng Gao. Ms-celeb-1m: A dataset and benchmark for large-scale face recognition. In *ECCV*, 2016. [2](#)

[25] Agrim Gupta, Piotr Dollar, and Ross Girshick. LVIS: A dataset for large vocabulary instance segmentation. In *CVPR*, 2019. 1, 2, 3, 5, 6, 9, 13, 15

[26] James Hays and Alexei A Efros. Scene completion using millions of photographs. *ACM Transactions on Graphics (TOG)*, 26(3):4–es, 2007. 6

[27] Haibo He and Edwardo A Garcia. Learning from imbalanced data. *IEEE Transactions on knowledge and data engineering*, 21(9):1263–1284, 2009. 2

[28] Haibo He and Edwardo A Garcia. Learning from imbalanced data. *IEEE Transactions on knowledge and data engineering*, 21(9):1263–1284, 2009. 5

[29] Kaiming He, Ross Girshick, and Piotr Dollár. Rethinking imagenet pre-training. In *ICCV*, 2019. 2

[30] Kaiming He, Georgia Gkioxari, Piotr Dollár, and Ross Girshick. Mask R-CNN. In *ICCV*, 2017. 1, 2, 8, 9, 13, 15

[31] Kaiming He, Xiangyu Zhang, Shaoqing Ren, and Jian Sun. Deep residual learning for image recognition. In *CVPR*, 2016. 1, 6, 13, 15

[32] Charles Herrmann, Chen Wang, Richard Strong Bowen, Emil Keyder, and Ramin Zabih. Object-centered image stitching. In *ECCV*, 2018. 2

[33] Judy Hoffman, Sergio Guadarrama, Eric S Tzeng, Ronghang Hu, Jeff Donahue, Ross Girshick, Trevor Darrell, and Kate Saenko. Lsda: Large scale detection through adaptation. In *NIPS*, 2014. 2

[34] Judy Hoffman, Deepak Pathak, Trevor Darrell, and Kate Saenko. Detector discovery in the wild: Joint multiple instance and representation learning. In *CVPR*, 2015. 2

[35] Judy Hoffman, Deepak Pathak, Eric Tzeng, Jonathan Long, Sergio Guadarrama, Trevor Darrell, and Kate Saenko. Large scale visual recognition through adaptation using joint representation and multiple instance learning. *JMLR*, 17(1):4954–4984, 2016. 2

[36] Xinting Hu, Yi Jiang, Kaihua Tang, Jingyuan Chen, Chunyan Miao, and Hanwang Zhang. Learning to segment the tail. In *CVPR*, 2020. 2, 8, 9, 15

[37] Sergey Ioffe and Christian Szegedy. Batch normalization: Accelerating deep network training by reducing internal covariate shift. In *ICML*, 2015. 4

[38] Jisoo Jeong, Seungeui Lee, Jeesoo Kim, and Nojun Kwak. Consistency-based semi-supervised learning for object detection. In *NeurIPS*, 2019. 2

[39] Bingyi Kang, Saining Xie, Marcus Rohrbach, Zhicheng Yan, Albert Gordo, Jiashi Feng, and Yannis Kalantidis. Decoupling representation and classifier for long-tailed recognition. In *ICLR*, 2020. 2, 5

[40] James Kirkpatrick, Razvan Pascanu, Neil Rabinowitz, Joel Veness, Guillaume Desjardins, Andrei A Rusu, Kieran Milan, John Quan, Tiago Ramalho, Agnieszka Grabska-Barwinska, et al. Overcoming catastrophic forgetting in neural networks. *PNAS*, 114(13):3521–3526, 2017. 8

[41] Ranjay Krishna, Yuke Zhu, Oliver Groth, Justin Johnson, Kenji Hata, Joshua Kravitz, Stephanie Chen, Yannis Kalantidis, Li-Jia Li, David A Shamma, et al. Visual genome: Connecting language and vision using crowdsourced dense image annotations. *IJCV*, 123(1):32–73, 2017. 2

[42] Alex Krizhevsky, Ilya Sutskever, and Geoffrey E Hinton. Imagenet classification with deep convolutional neural networks. In *NIPS*, 2012. 1

[43] Jason Kuen, Federico Perazzi, Zhe Lin, Jianming Zhang, and Yap-Peng Tan. Scaling object detection by transferring classification weights. In *ICCV*, 2019. 2

[44] Alina Kuznetsova, Hassan Rom, Neil Alldrin, Jasper Uijlings, Ivan Krasin, Jordi Pont-Tuset, Shahab Kamali, Stefan Popov, Matteo Mallocci, Alexander Kolesnikov, et al. The open images dataset v4. *IJCV*, pages 1–26, 2020. 1

[45] Dong-Hyun Lee. Pseudo-label: The simple and efficient semi-supervised learning method for deep neural networks. In *ICML Workshop*, 2013. 6

[46] Dong Li, Jia-Bin Huang, Yali Li, Shengjin Wang, and Ming-Hsuan Yang. Weakly supervised object localization with progressive domain adaptation. In *CVPR*, 2016. 2, 5

[47] Yandong Li, Di Huang, Danfeng Qin, Liqiang Wang, and Boqing Gong. Improving object detection with selective self-supervised self-training. In *ECCV*, 2020. 2, 5

[48] Yu Li, Tao Wang, Bingyi Kang, Sheng Tang, Chunfeng Wang, Jintao Li, and Jiashi Feng. Overcoming classifier imbalance for long-tail object detection with balanced group softmax. In *CVPR*, 2020. 1, 2, 8, 15

[49] Tsung-Yi Lin, Piotr Dollár, Ross Girshick, Kaiming He, Bharath Hariharan, and Serge Belongie. Feature pyramid networks for object detection. In *CVPR*, 2017. 1, 6, 15

[50] Tsung-Yi Lin, Priya Goyal, Ross Girshick, Kaiming He, and Piotr Dollár. Focal loss for dense object detection. In *ICCV*, 2017. 1

[51] Tsung-Yi Lin, Michael Maire, Serge Belongie, James Hays, Pietro Perona, Deva Ramanan, Piotr Dollár, and C Lawrence Zitnick. Microsoft COCO: Common objects in context. In *ECCV*, 2014. 1, 2, 3, 15

[52] Wei Liu, Dragomir Anguelov, Dumitru Erhan, Christian Szegedy, Scott Reed, Cheng-Yang Fu, and Alexander C Berg. Ssd: Single shot multibox detector. In *ECCV*, 2016. 1, 2

[53] George A Miller. WordNet: A lexical database for english. *Communications of the ACM*, 38(11):39–41, 1995. 3, 5, 6, 15

[54] Constantine P Papageorgiou, Michael Oren, and Tomaso Poggio. A general framework for object detection. In *ICCV*, 1998. 1

[55] Vignesh Ramanathan, Rui Wang, and Dhruv Mahajan. DLWL: Improving detection for lowshot classes with weakly labelled data. In *CVPR*, 2020. 2, 5, 6, 8, 9

[56] Joseph Redmon, Santosh Divvala, Ross Girshick, and Ali Farhadi. You only look once: Unified, real-time object detection. In *CVPR*, 2016. 1

[57] Joseph Redmon and Ali Farhadi. Yolo9000: better, faster, stronger. In *CVPR*, 2017. 2

[58] Jiawei Ren, Cunjun Yu, Shunan Sheng, Xiao Ma, Haiyu Zhao, Shuai Yi, and Hongsheng Li. Balanced meta-softmax for long-tailed visual recognition. In *NeurIPS*, 2020. 2, 8, 9, 15

[59] Shaoqing Ren, Kaiming He, Ross Girshick, and Jian Sun. Faster R-CNN: Towards real-time object detection with region proposal networks. In *NIPS*, 2015. 1, 3, 4, 6, 13, 15

[60] Olga Russakovsky, Jia Deng, Hao Su, Jonathan Krause, Sanjeev Satheesh, Sean Ma, Zhiheng Huang, Andrej Karpathy, Aditya Khosla, Michael Bernstein, et al. Imagenet large scale visual recognition challenge. *IJCV*, 115(3):211–252, 2015. [2](#), [3](#), [6](#), [15](#)

[61] Shuai Shao, Zeming Li, Tianyuan Zhang, Chao Peng, Gang Yu, Xiangyu Zhang, Jing Li, and Jian Sun. Objects365: A large-scale, high-quality dataset for object detection. In *ICCV*, 2019. [1](#), [3](#)

[62] Karen Simonyan and Andrew Zisserman. Very deep convolutional networks for large-scale image recognition. In *ICLR*, 2015. [1](#)

[63] Kihyuk Sohn, Zizhao Zhang, Chun-Liang Li, Han Zhang, Chen-Yu Lee, and Tomas Pfister. A simple semi-supervised learning framework for object detection. *arXiv preprint arXiv:2005.04757*, 2020. [2](#)

[64] Christian Szegedy, Wei Liu, Yangqing Jia, Pierre Sermanet, Scott Reed, Dragomir Anguelov, Dumitru Erhan, Vincent Vanhoucke, and Andrew Rabinovich. Going deeper with convolutions. In *CVPR*, 2015. [1](#)

[65] Jingru Tan, Changbao Wang, Buyu Li, Quanquan Li, Wanli Ouyang, Changqing Yin, and Junjie Yan. Equalization loss for long-tailed object recognition. In *CVPR*, 2020. [1](#), [2](#), [5](#), [8](#), [9](#), [15](#)

[66] Jingru Tan, Gang Zhang, Hanming Deng, Changbao Wang, Lewei Lu, Quanquan Li, and Jifeng Dai. 1st place solution of lvis challenge 2020: A good box is not a guarantee of a good mask. *arXiv preprint arXiv:2009.01559*, 2020. [15](#)

[67] Kaihua Tang, Jianqiang Huang, and Hanwang Zhang. Long-tailed classification by keeping the good and removing the bad momentum causal effect. In *NeurIPS*, 2020. [2](#)

[68] Yuxing Tang, Josiah Wang, Boyang Gao, Emmanuel Dellandréa, Robert Gaizauskas, and Liming Chen. Large scale semi-supervised object detection using visual and semantic knowledge transfer. In *CVPR*, 2016. [2](#)

[69] Yuxing Tang, Josiah Wang, Xiaofang Wang, Boyang Gao, Emmanuel Dellandréa, Robert Gaizauskas, and Liming Chen. Visual and semantic knowledge transfer for large scale semi-supervised object detection. *TPAMI*, 40(12):3045–3058, 2017. [2](#)

[70] Bart Thomee, David A Shamma, Gerald Friedland, Benjamin Elizalde, Karl Ni, Douglas Poland, Damian Borth, and Li-Jia Li. YFCC100M: The new data in multimedia research. *Communications of the ACM*, 59(2):64–73, 2016. [1](#), [2](#), [6](#), [8](#), [9](#)

[71] Jasper Uijlings, Stefan Popov, and Vittorio Ferrari. Revisiting knowledge transfer for training object class detectors. In *CVPR*, 2018. [2](#), [5](#)

[72] Grant Van Horn, Oisin Mac Aodha, Yang Song, Yin Cui, Chen Sun, Alex Shepard, Hartwig Adam, Pietro Perona, and Serge Belongie. The inaturalist species classification and detection dataset. In *CVPR*, pages 8769–8778, 2018. [1](#), [2](#)

[73] Paul Viola, Michael Jones, et al. Robust real-time object detection. *IJCV*, 4(34–47):4, 2001. [1](#)

[74] Jiaqi Wang, Wenwei Zhang, Yuhang Zang, Yuhang Cao, Jiangmiao Pang, Tao Gong, Kai Chen, Ziwei Liu, Chen Change Loy, and Dahua Lin. Seesaw loss for long-tailed instance segmentation. *arXiv preprint arXiv:2008.10032*, 2020. [15](#)

[75] Tao Wang, Yu Li, Bingyi Kang, Junnan Li, Junhao Liew, Sheng Tang, Steven Hoi, and Jiashi Feng. The devil is in classification: A simple framework for long-tail instance segmentation. In *ECCV*, 2020. [2](#), [9](#)

[76] Xin Wang, Thomas E Huang, Trevor Darrell, Joseph E Gonzalez, and Fisher Yu. Frustratingly simple few-shot object detection. In *ICML*, 2020. [1](#), [2](#), [8](#), [15](#)

[77] Zirui Wang, Zihang Dai, Barnabás Póczos, and Jaime Carbonell. Characterizing and avoiding negative transfer. In *CVPR*, 2019. [2](#), [3](#)

[78] Jialian Wu, Liangchen Song, Tiancai Wang, Qian Zhang, and Junsong Yuan. Forest R-CNN: Large-vocabulary long-tailed object detection and instance segmentation. In *ACM MM*, 2020. [2](#), [9](#), [15](#)

[79] Han-Jia Ye, Hong-You Chen, De-Chuan Zhan, and Wei-Lun Chao. Identifying and compensating for feature deviation in imbalanced deep learning. *arXiv preprint arXiv:2001.01385*, 2020. [5](#)

[80] Fisher Yu, Haofeng Chen, Xin Wang, Wenqi Xian, Yingying Chen, Fangchen Liu, Vashisht Madhavan, and Trevor Darrell. BDD100K: A diverse driving dataset for heterogeneous multitask learning. In *CVPR*, 2020. [1](#), [3](#)

[81] Sangdoo Yun, Dongyoon Han, Seong Joon Oh, Sanghyuk Chun, Junsuk Choe, and Youngjoon Yoo. Cutmix: Regularization strategy to train strong classifiers with localizable features. In *ICCV*, 2019. [2](#)

[82] Amir R Zamir, Alexander Sax, William Shen, Leonidas J Guibas, Jitendra Malik, and Silvio Savarese. Taskonomy: Disentangling task transfer learning. In *CVPR*, 2018. [2](#), [3](#)

[83] Fan Zhang and Feng Liu. Parallax-tolerant image stitching. In *CVPR*, 2014. [6](#)

[84] Hongyi Zhang, Moustapha Cisse, Yann N Dauphin, and David Lopez-Paz. mixup: Beyond empirical risk minimization. In *ICLR*, 2017. [2](#)

[85] Yubo Zhang, Pavel Tokmakov, Martial Hebert, and Cordelia Schmid. A study on action detection in the wild. *arXiv preprint arXiv:1904.12993*, 2019. [2](#)

[86] Zhi Zhang, Tong He, Hang Zhang, Zhongyue Zhang, Junyuan Xie, and Mu Li. Bag of freebies for training object detection neural networks. *arXiv preprint arXiv:1902.04103*, 2019. [2](#)

[87] Xiangxin Zhu, Dragomir Anguelov, and Deva Ramanan. Capturing long-tail distributions of object subcategories. In *CVPR*, pages 915–922, 2014. [1](#)

[88] Barret Zoph, Ekin D Cubuk, Golnaz Ghiasi, Tsung-Yi Lin, Jonathon Shlens, and Quoc V Le. Learning data augmentation strategies for object detection. *arXiv preprint arXiv:1906.11172*, 2019. [2](#)

[89] Barret Zoph, Golnaz Ghiasi, Tsung-Yi Lin, Yin Cui, Hanxiao Liu, Ekin Dogus Cubuk, and Quoc Le. Rethinking pre-training and self-training. In *NeurIPS*, 2020. [1](#), [2](#)

Supplementary Material

In this supplementary material, we provide details and results omitted in the main text.

- **Appendix A:** details on LORE (localization by region removal) (subsection 5.2 of the main text).
- **Appendix B:** details on instance segmentation (subsection 6.3 of the main paper).
- **Appendix C:** additional ablation studies (subsection 6.2 of the main paper).
- **Appendix D:** comparison to state-of-the-art methods (subsection 6.2 of the main paper).
- **Appendix E:** results on LVIS v1.0 dataset (subsection 6.2 and subsection 6.3 of the main paper).
- **Appendix F:** additional qualitative results (subsection 6.2 of the main paper).

A. Details on LORE

Figure 7 shows the pipeline of localization by region removal (LORE), which is introduced in section 5.2 of the main paper for pseudo-label generation. Concretely, LORE takes an object-centric image as the input and identifies the locations of the target object (*i.e.*, that of image label) in the image. The whole pipeline consists of three major components: (1) classifier training, (2) box pre-filtering, and (3) localization by removal. We describe each step as follows.

Classifier training. We train a ResNet-50 [31] image classifier with all object-centric images. For LVIS v0.5 dataset, we follow the conventional training procedure⁸ to train a 1,230-way ResNet classifier. Specifically, we train the networks with 90 epoch and achieve 74% top-1 training accuracy. We use the well-trained classifier for selecting high-confidential regions in the object-centric image.

Box pre-filtering. We feed an object-centric image into the pre-trained *object detector* and collect detection results. Concretely, we take the top 300 final predictions of faster-RCNN [59] and drop each box’s predicted class label. Next, we apply non-maximum suppression (NMS) over all the 300 boxes using a threshold of 0.5 to remove highly-overlapped ones. Basically, we trust the detected box locations (that they do contain some objects), but will recheck which of them belongs to the target object.

⁸<https://github.com/pytorch/examples/tree/master/imagenet>

To further reduce the number of candidate boxes, we sort the boxes by their initial detection confidence (in the descending order) and then remove them *in turn*⁹, every time followed by applying the image classifier to the resulting image. We stop this process until the classification confidence of the target class goes below a certain threshold. We then collect the removed box locations, which together have likely covered the target objects (high recall, but likely low precision), to be the candidate box pool for the next step.

Localization by removal. To accurately identify which candidate truly belongs to the target class, we *re-rank* the candidates by how much removing each boxed region *alone* reduces the image classifier’s confidence on the target class. We then follow the descending order to remove these boxed regions *in turn* until the classifier fail to predict the target class or the *reducing ratio*¹⁰ achieves a certain threshold. Finally, the bounding boxes of the removed regions are collected as the pseudo ground-truths of the target class for the image. More examples can be found in Figure 8.

B. Details on Instance Segmentation

Background on instance segmentation. We apply mask-RCNN [30], which adopts the same two-stage procedure similar to faster-RCNN [59], with an identical first stage RPN. In the second stage, in addition to predicting the class label and box offset, mask R-CNN also outputs a binary segmentation mask for each proposal. Formally, during training, the entire mask R-CNN is learned with four loss terms

$$\mathcal{L} = \mathcal{L}_{\text{rpn}} + \mathcal{L}_{\text{cls}} + \mathcal{L}_{\text{reg}} + \mathcal{L}_{\text{mask}}, \quad (2)$$

where the RPN loss \mathcal{L}_{rpn} , classification loss \mathcal{L}_{cls} and box regression loss \mathcal{L}_{reg} are identical to those defined in [59]. The mask loss $\mathcal{L}_{\text{mask}}$ is learned via an average binary cross-entropy objective.

Multi-stage training for instance segmentation. We first train a mask-RCNN using labeled scene-centric images with instance segmentation annotations [25]. All the four loss terms in Equation 2 are optimized.

We then fine-tune the model using the pseudo scene-centric images that are generated from object-centric images. Concretely, we use these images (only with box labels) to fine-tune the model using \mathcal{L}_{cls} . In other words, we do not optimize \mathcal{L}_{rpn} , \mathcal{L}_{reg} , and $\mathcal{L}_{\text{mask}}$. Again, any network parameters that affect \mathcal{L}_{cls} , especially those in the backbone feature network, can be updated.

⁹Cropping out the corresponding image regions and replacing them by gray-color patches

¹⁰We define the *reducing ratio* as the relative confidence drop on the target class label before and after removing boxes.

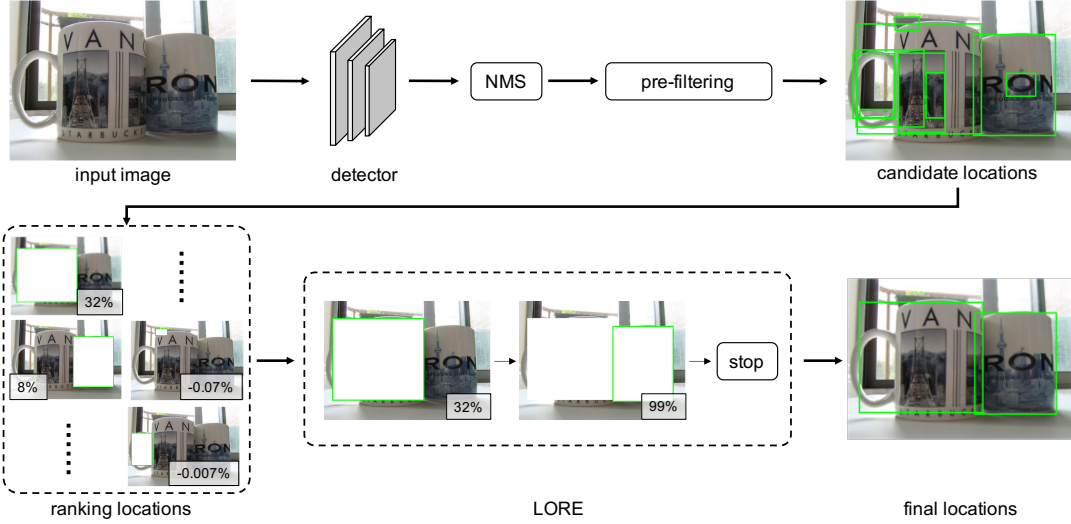


Figure 7. **Illustration of LORE.** We first apply a pre-trained detector to obtain candidate boxes, followed by pre-filtering. We then sort the remaining boxes using an image classifier. Finally, we remove the boxes in turn until the classifier fail to predict the target image label. The numbers at image corners indicate the confidence reducing ratio. Negative values mean the confidence increases after removing outliers.

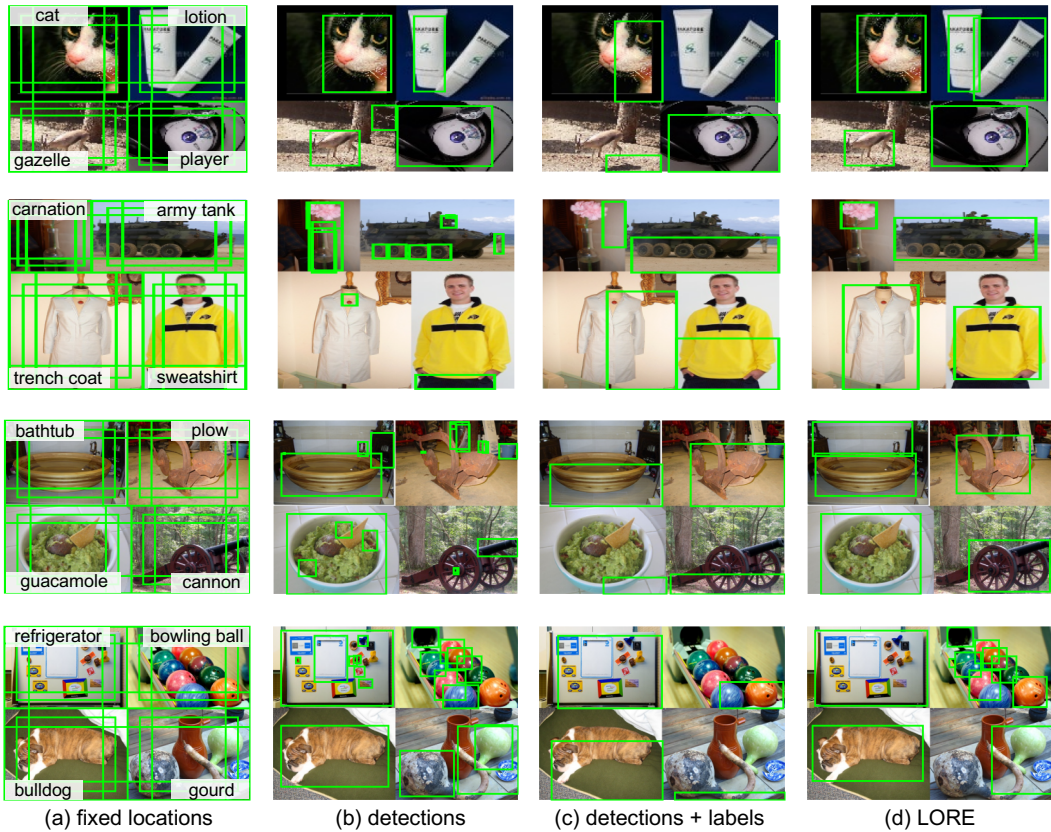


Figure 8. **More examples of pseudo-scene-centric images.** We show (a) fixed locations, (b) trust the detector, (c) trust the detector + image labels, and (d) localization by region removals (LORE). The green boxes are the pseudo ground-truth locations found on each object-centric image alone before multiple images are stitched together. We can see that LORE accurately locates the target object in each sub-image while detection results are much noisy. Each box is assigned with the image label except (b), which takes detection labels. Image labels are listed on the corner of each sub-image.

Table 6. **Comparison of different types of mosaic images.** Here we use ImageNet-21K as the source of object-centric images and stitch images from the same class and use the 6 fixed locations as pseudo ground-truths. 1×1 OCI means directly using the original object-centric images. Results are reported on LVIS v0.5 val. We can see that 2×2 mosaic gives better performance on all classes. The best result per column is in bold font.

Layout	AP ^b	AP _r ^b	AP _c ^b	AP _f ^b
faster RCNN*	23.35	12.98	22.60	28.42
1×1 OCI	23.81	15.18	22.91	28.39
3×3 Mosaic	24.32	17.90	23.01	28.51
2×2 Mosaic	24.42	18.15	23.12	28.56

After this stage, we fine-tune the whole network again with labeled scene-centric images, just like the first stage. Different from object detection, we also include pixel annotations for instance segmentation: all the four loss terms in [Equation 1](#) are optimized.

C. Additional Ablation Studies

C.1. Effects of image stitching

We investigate the effect of different types of layouts for stitching object-centric images, *i.e.*, 1×1 (which is the original object-centric image), 2×2 mosaic, and 3×3 mosaic. We show examples of 2×2 and 3×3 mosaics in [Figure 9](#). We evaluate them under the same experimental settings: we use ImageNet-21K as the source of object-centric images (1,016 classes) and stitch images from the same class and use the 6 fixed locations as pseudo ground-truths. [Table 6](#) shows the comparison of object detection results on LVIS v0.5 dataset. We see that 2×2 and 3×3 mosaics perform similarly and both outperform the 1×1 OCI (on AP^b).

D. Comparison to State-of-the-art Methods

We compare our approach with the state-of-the-art methods in details. We note that, beyond those introduced in the baseline LVIS models [25], we do not apply any new objective functions or learning strategies to train the detector with LVIS images. As shown in the [Table 4](#) and [Table 5](#) of the main text, our method outperforms EQL [65], LST [36], TFA [76], Forest RCNN [78] on all classes without additional training strategies and data augmentations. We note that, achieving state-of-the-art results usually needs detailed tuning. For instance, BAGS [48] model is pre-trained on COCO [51] while our model is initialized from ResNet-50 pre-trained on ImageNet-1K (ILSVRC). Moreover, when combined with [58], our approach achieves state-of-the-art performance on LVIS v0.5 object detection and instance segmentation. We expect that our framework can be further improved by incorporating more advanced learning strategies [48, 76, 58, 66, 74] on long-tailed object recognition.

E. Experimental Results on LVIS v1.0

E.1. Setup

Dataset statistics. We further evaluate our proposed method on LVIS v1.0 dataset [25]. The total dataset size has been expanded to ~ 160 K images and ~ 2 M instance annotations. The total number of categories has decreased slightly (from 1230 to 1203) due to more stringent quality control. More specifically, LVIS v1.0 adds 52 new classes while drops 79 classes from LVIS v0.5. The validation set has been expanded from 5K images to 20K images. [Table 8](#) gives a summary of the statistics of the two versions of LVIS dataset. We follow the experimental setups of LVIS v0.5 to use category synset ID [53] to search for the corresponding classes in ImageNet-21K dataset [60]. In total, we collect 753,700 object-centric images. [Table 7](#) shows the detailed statistics of the number of overlapped classes in those datasets. As supplements, we also search 100 images for other classes via Google Images.

Baseline. For object detection, we use **faster-RCNN** [59] as our base detector and ResNet-50 [31] with a Feature Pyramid Network (FPN) [49] as the backbone, which is pre-trained on ImageNet-1K [60]. We use repeated factor sampling, following the standard training procedure in [25]. No additional data augmentation techniques are used. Specifically, we train the baseline for 180K iterations with a mini-batch size of 16 and an initial learning rate of 0.02. The learning rate is decayed by 10 at 120K and 160K iterations, respectively. We further extend the training process with another 180K iterations to select the checkpoint with the best AP^b as our base detector. For instance segmentation, we use **mask-RCNN** [30] with instance segmentation annotations. The training scheme is the same with training faster-RCNN for object detection.

Our settings. Following our multi-stage pipeline, we first fine-tune the base detector for 90K iterations with pseudo scene-centric-images using only the classification loss. Our pseudo scene-centric-images are synthesized with 2×2 mosaic from random classes of ImageNet-21K and Google images. For Google, we also retrieve top 100 images for each of the 1,203 classes. We use the boxes with 6 fixed locations as pseudo ground-truths. After that, we end-to-end fine-tune the entire model for another 180K iterations using the LVIS training set with all losses. Following [subsection 6.1](#), all steps are trained with stochastic gradient descent with a mini-batch size of 16, momentum of 0.9, weight decay of 0.0001, and learning rate of 0.0002.

E.2. Results on LVIS v1.0 object detection

We first show object detection results on LVIS v1.0 dataset in [Table 9](#). We see similar observations as in LVIS



Scene-Centric Image in LVIS

2 x 2 Mosaic

3 x 3 Mosaic

Figure 9. **Different layouts of mosaics.** We show different types of images from the same category (**windmill**). We can find that the 2×2 mosaic image (middle) and the real scene-centric image (left) in the LVIS dataset look-alike in terms of appearance and structure while the 3×3 mosaic image (right) is much crowded.

Table 7. **Number of overlapped classes in LVIS and ImageNet.** In LVIS and ImageNet, each category can be identified by a unique WordNet synset ID. We match LVIS classes to ImageNet ones and show the number of the overlapped classes. Specifically, we show # LVIS classes / # overlapped to ImageNet-21K / # overlapped to ImageNet-1K (ILSVRC).

Version	Split	Frequent	Common	Rare	Overall
v0.5	Train	315 / 253 / 85	461 / 387 / 96	454 / 385 / 71	1230 / 1025 / 252
	Val	313 / 252 / 21	392 / 329 / 84	125 / 106 / 71	830 / 678 / 176
v1.0	Train	405 / 331 / 87	461 / 390 / 96	337 / 277 / 64	1203 / 998 / 247
	Val	405 / 331 / 87	452 / 382 / 92	178 / 144 / 37	1035 / 857 / 216

Table 8. **Statistics of LVIS v0.5 and v1.0 datasets.**

Version	Type	Train	Val	Test
v0.5	# Image	57,263	5,000	19,761
	# Class	1,230	830	-
	# Instance	693,958	50,763	-
v1.0	# Image	100,170	19,809	19,822
	# Class	1,203	1,035	-
	# Instance	1,270,141	244,707	-

Table 9. **Object detection on LVIS v1.0.** Our approach largely outperforms the base detector on all classes.

Method	AP ^b	AP ₅₀ ^b	AP ₇₅ ^b	AP _r ^b	AP _c ^b	AP _f ^b
Baseline	22.01	36.36	23.14	10.57	20.09	29.18
Ours	23.33	38.58	24.23	14.23	21.67	29.18

v0.5. Our approach outperforms the baseline detector substantially by leveraging object-centric images to compensate long-tailed distribution. Overall we improve 1.3% AP^b. More importantly, we achieve 14.23% on rare classes, which is nearly 4% higher than that by the baseline detector. We also improve common classes from 20.09% to 21.67%, without sacrificing frequent classes.

E.3. Results on LVIS v1.0 instance segmentation

Table 10 shows results on instance segmentation. Our approach outperforms the baseline detector especially for

Table 10. **Instance segmentation on LVIS v1.0.** Our approach largely outperforms the base detector on all classes.

Method	Backbone	AP	AP ₅₀	AP ₇₅	AP _r	AP _c	AP _f
Baseline	R-50	22.59	35.44	23.87	12.31	21.30	28.55
Ours	R-50	24.11	37.63	25.27	17.12	22.70	28.78
Baseline	X-101	26.62	40.47	28.29	17.51	25.51	31.86
Ours	X-101	28.31	42.92	30.65	21.74	27.25	32.36

rare classes. With the ResNet-50 backbone, we achieve 24.11% on AP^b and 17.12% on AP_r^b, better than the base detector. We also report segmentation results based on stronger backbone and observe similar trends.

F. Additional Qualitative Results

In this section, we show additional qualitative results on LVIS v0.5 object detection in Figure 10. We compare the ground truth, the results of baseline and the results of our method. Interestingly, we observe that our method can accurately recognize the objects from rare categories that may be overlooked by the baseline detector. Moreover, the results demonstrate that our approach is able to correct the prediction labels that were wrongly classified to frequent ones, without sacrificing the detection performance on common and frequent classes.

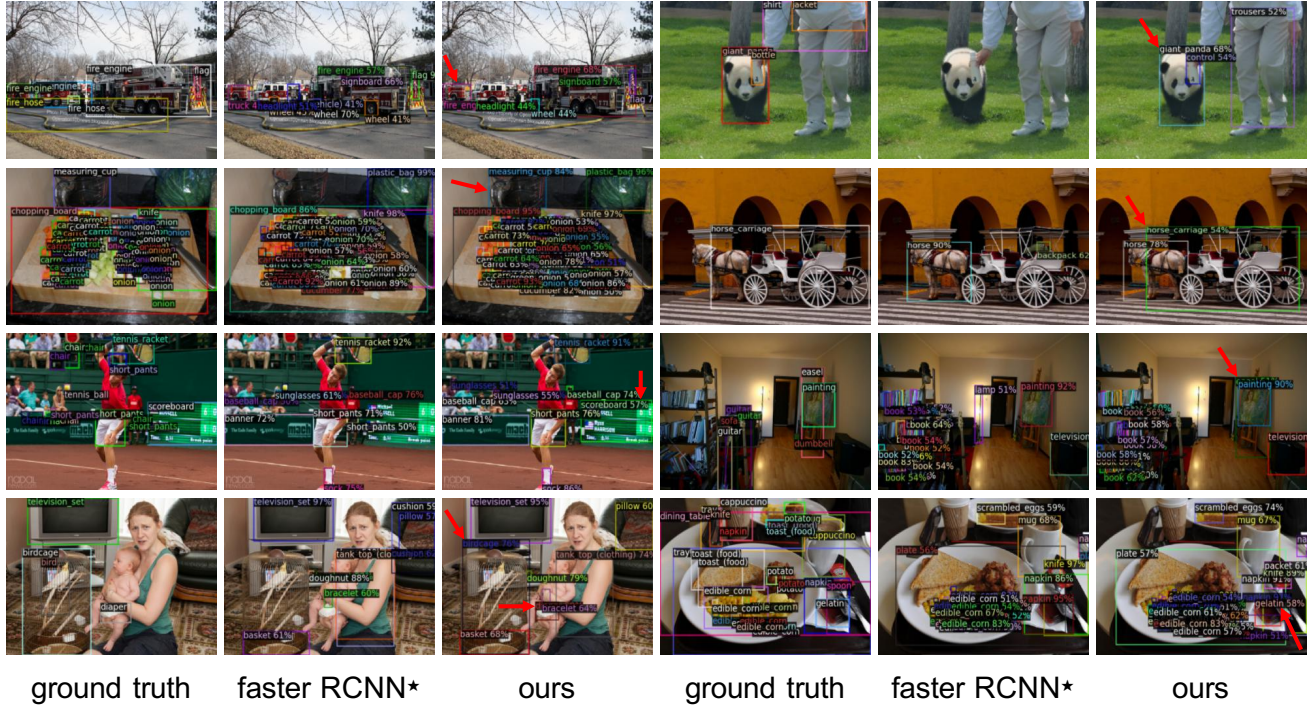


Figure 10. **Qualitative results.** Our approach can detect rare objects that may be overlooked (e.g., *measuring cup*, *giant panda*) by the baseline detector and correct the labels that were wrongly classified to frequent categories (e.g., predict *fire engine* instead of *truck*). We superimpose red arrows to show where we did right while the baseline did wrong. Zoom in for details.